Title	Effects of Biomass Type, Carbonization Process, and Activation Method on the Properties of Bio-Based Activated Carbons
Author(s)	Siipola, V., Tamminen, T., Källi, A., Lahti, R., Romar, H., Rasa, K., Keskinen, R., Hyväluoma, J., Hannula, M., Wikberg, H.
Citation	BioResources, vol.11, issue 3 (2018)
Date	24.10.2018
DOI	10.15376/biores.13.3.5976-6002
Rights	This article may be downloaded for personal use only.

Effects of Biomass Type, Carbonization Process, and Activation Method on the Properties of Bio-Based Activated Carbons

Virpi Siipola,[a,*] Tarja Tamminen,[a] Anssi Källi,[a] Riikka Lahti,[b] Henrik Romar,[b] Kimmo Rasa,[c] Riikka Keskinen,[c] Jari Hyväluoma,[c] Markus Hannula,[d] and Hanne Wikberg [a]

Activated carbons (AC) serve as adsorbents in various applications requiring specific functionalities. In this study, the effects of biomass type, pre-carbonization process, and activation method on the properties of ACs were investigated. Chemical (KOH and H_3PO_4) and physical (CO_2) activations were performed on slow pyrolyzed and hydrothermally carbonized (HTC) biochars produced from two feedstocks, willow and Scots pine bark (SPB). In addition, the adsorption capacities of the ACs were tested with two dyes and zinc metal. Distinct differences were found between the biochars and ACs regarding pore size distributions, surface area (238 - 3505 m^2 g^{-1}), and surface chemistry. KOH activation produced highly microporous ACs from all biochars, whereas with H_3PO_4 and CO_2 there was also increase in the meso- and macroporosity with the HTC biochars. Adsorption capacity for dyes was dependent on the surface area, while for zinc it depended on AC's pH. The results provide interesting insights into tailoring ACs for specific applications.

Keywords: Biochar; Activated carbon; Bio-based activated carbon; Willow; Pine bark; X-ray tomography

*Contact information: a: VTT Technical Research Centre of Finland Ltd, P.O.Box 1000, FI-02044 VTT, Espoo, Finland; b: University of Oulu, Research Unit of Sustainable Chemistry, P.O. Box 3000, FI-90014 University of Oulu, Finland; c: Natural Resources Institute Finland (Luke), FI-31600 Jokioinen, Finland; d: BioMediTech Institute and Faculty of Biomedical Sciences and Engineering, Tampere University of Technology, Tampere, Finland; *Corresponding author: virpi.siipola@vtt.fi*

INTRODUCTION

Activated carbons (ACs) are widely used as adsorbents in numerous applications, as they possess high surface area and porosity, and in theory, they can be produced from any raw material with high carbon content and, preferably, low amount of inorganic compounds (Marsh and Rodríguez-Reinoso 2006; Ioannidou and Zabaniotou 2007). In practice, industrial ACs are prepared from quite a few raw materials, which fulfill the reliability and constancy needed for large-scale production. Such raw materials include *e.g*., coal, peat, some woods, fruits, and nutshells (Marsh and Rodríguez-Reinoso 2006). The global production of ACs is increasing as new, stricter environmental regulations for air and water purification especially in the Western Europe and Canada are implemented. Simultaneously the demand coming from developing countries in Asia and Africa is rising. The development of bioeconomy has directed focus in AC production for utilizing lignocellulosic side-streams from agro- and forest industries. The suitability of various raw materials, working procedures and potential adsorption applications are constantly being tested and further developed (Ioannidou and Zabaniotou 2007; Jain *et al*. 2016).

Chemical and physical activations are often conducted directly on the biomass, but biochars provide an interesting option, as pre-carbonization of biomass has been shown to increase activation yields and surface area due to enhanced microporosity (Basta *et al.* 2009). The low yields and pore development resulting from biomass activation is due to excessive degradation of organic matter, whereas biochars resemble more traditional coal precursors and are therefore more suitable for higher porosity development (Basta *et al.* 2009; Falco *et al.* 2013). In this study, slow pyrolyzed and hydrothermally carbonized biochars were used as raw materials for activations. Slow pyrolysis (SP) is a thermochemical conversion process performed under low oxygen or preferably inert atmosphere at elevated temperatures (*e.g.*, 300 to 650 °C) to produce biochar. SP uses lower temperatures and longer residence times compared to other pyrolysis methods (fast, flash), where main products are liquid and non-condensable gases. By modifying the heating rate and temperature, biochars with different qualities in respect to carbon content, surface area and heating value, for instance, can be produced (Kambo *et al.* 2015). Hydrothermal carbonization (HTC) has received much attention during recent years as a sustainable, straightforward and easily scalable thermochemical conversion process that is suitable for wet biomass and thus excludes the need for biomass drying prior to carbonization. During HTC processing, organic raw material is carbonized in water at moderate temperatures (180 to 260 °C) under self-generated pressures (< 50 bar) for a few hours (Wikberg *et al*. 2015a; 2015b). In the process, wet feedstock is converted into carbonaceous material in a form of solid biochar, often called hydrochar. Other products include non-condensable gases (mostly CO_2) and small aqueous degradation products (*e.g.*, residues, sugars, organic acids) together with water. One of the benefits of HTC is that the lower temperatures do not destroy the porous structures of the biomass as much as pyrolysis operated at higher temperatures (Ioannidou and Zabaniotou 2007). In addition, HTC biochars have high amounts of surface oxygen groups (SOG), which make them attractive candidates for highly surface-active ACs (Kambo *et al*. 2015; Jain *et al*. 2016).

Activation of biochar or biomass is performed using either physical or chemical activation methods. Physical activation is usually performed at high temperatures up to 1000 °C by using steam or CO_2 as activation gas or by combining these two (Yahya *et al*. 2015). The quality of the produced AC (*e.g.*, the surface area and porosity) is a sum of many factors, such as the type of the raw material, activation gas, temperature, and time. In chemical activation, the surface area and porosity are introduced inside the carbon by impregnating the raw material by desired chemical, followed by thermal treatment at temperatures typically between 300 and 800 °C (Ioannidou and Zabaniotou 2007).

Many impregnation chemicals have been tested for the chemical activations, producing very high surface areas above 3000 m^2 g^{-1} (Ioannidou and Zabaniotou 2007; Yahya *et al*. 2015; Jain *et al*. 2016). The chemical is chosen depending on the end application (Jain *et al.* 2016) or the raw material type. Phosphoric acid (H_3PO_4) is commonly used for lignocellulosic materials starting from biomass (Jagtoyen and Derbyshire 1998; Romero-Anaya *et al.* 2012) and alkaline chemicals (*e.g.*, KOH) for the activation of coals or biochars (Lozano-Castelló *et al.* 2001). The phosphoric acid produces, in general, more mesoporous AC than KOH activation, although the activation result depends highly on the raw material used (Romero-Anaya *et al.* 2012). Chemical activation usually produces higher surface areas than physical activation as the used impregnation chemicals inhibit the formation of tar and reduce the number of other volatile products (Lozano-Castelló *et al*. 2001). The downsides of the chemical activation are the laborious working procedure that requires washing of the end product and the

corrosiveness of the chemicals which wears the equipment (Lozano-Castelló *et al.* 2001). Finding the optimal activation conditions usually requires long test series with varying time, temperature, activation chemical, gas, and flow rates. The difficulty in finding optimal activation conditions to produce desired AC qualities is in the heterogeneity of the biomass. The original pore structure of the plant affects the resulting pore structure especially with milder activation temperatures. The amount of lignin and the variety of chemical compounds in the plant tissue also play a role in the porosity and surface activity development.

The main focus in AC manufacturing has been shifted from producing the highest possible surface areas into other qualifications for a multitude of different applications. Tailoring the pore structure toward certain pore size distributions (PSD) is beneficial in electrochemical applications, such as supercapacitors or in gas storage applications (Sevilla and Mokaya 2014). Biochar also performs well in fuel cell applications (Munnings *et al*. 2014; Cai *et al*. 2016). Biomass selection plays a vital role in these types of applications. For example, plant-derived biochars containing naturally existing heteroatoms are beneficial in direct carbon oxide fuel cell applications (Cai *et al*. 2016).

In order to produce activated carbons that achieve high performance in a selected application, process optimization on the selected feedstock has to be performed. This optimization has to be performed keeping the final use of the carbons produced in mind. The results presented in this study can be regarded as a pre-screening of feedstock and procedures prior to more detailed process optimization.

In this study, two raw materials, scots pine bark (SPB) and willow, were used to produce chemically and physically activated carbons from slow pyrolyzed and hydrothermally carbonized biochars using activation conditions selected on the basis of thermogravimetric pre-experiments and literature (Fig. 1). These biomasses were selected because willow grows fast and can be cultivated as an energy plant; pine bark waste, on the other hand, is produced in vast quantities in saw mills as well as in the pulp and paper industry. Despite the large quantities of these boreal biomasses annually produced, their utilization for higher value products, such as activated carbons, has been scarce. Also, comparisons between slow pyrolysis and HTC pre-carbonized bio-based activated carbons in regard surface properties produced under similar activation conditions, are few. The samples were characterized for their elemental composition, BET surface area, porosity and adsorption capacity. Surface qualities were analyzed using FT-IR and Boehm titration. In addition, X-ray tomography and image analysis were used to quantitatively analyze micron-scale porosity of one of the samples. To our knowledge, this is the first time that X-ray tomography has been used to evaluate influence of chemical activation on skeleton structure of hydrothermally carbonized biomass. The goal of this work was to understand the effects of the biomass type, pre-carbonization process, and activation method on the properties of ACs. The qualities of the produced ACs are also discussed with regard to potential applications.

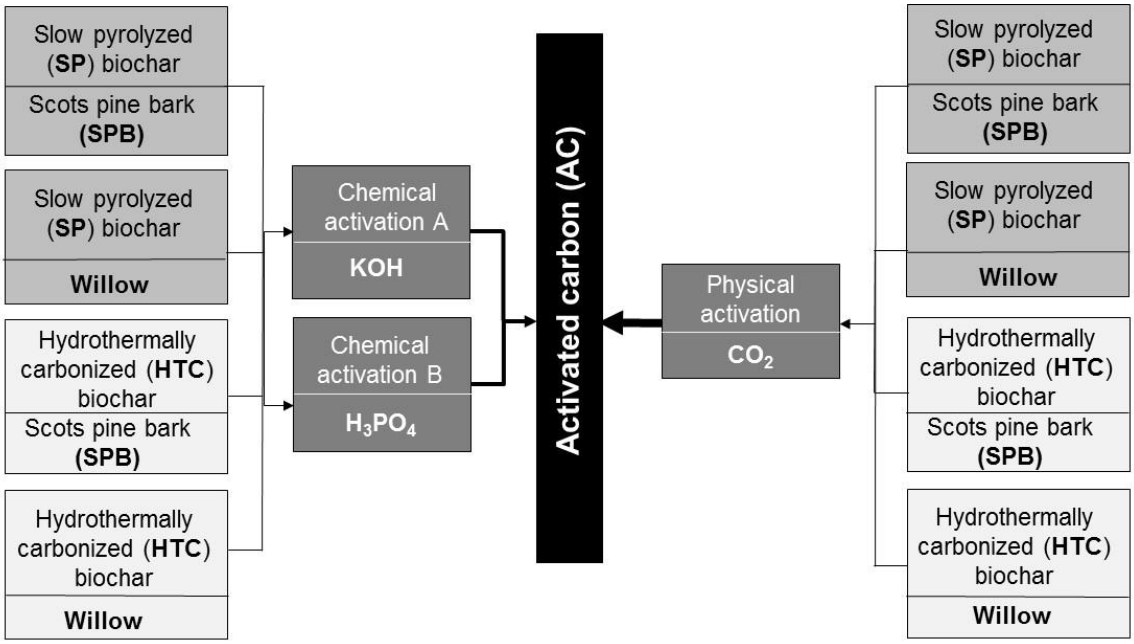

Fig. 1. Activation procedures

EXPERIMENTAL

Materials

Scots pine bark (SPB) and willow (*Salix* sp., unbarked short rotation coppice) were acquired from Sweden and dried at < 70 °C in a flat-bed drying wagon with forced ventilation prior to shredding using a single-shaft shredder (Lindner Micromat 2000, Lindner-Recyclingtech GmbH, Spittal, Austria) with a 15 mm screen. The raw materials were carbonized using either slow pyrolysis (SP) at 475 °C for 3 h or HTC at 260 °C for 6 h, resulting in four different types of biochars (Fig. 1). A detailed description of the carbonization experiments is available elsewhere (Keskinen *et al.* 2017; Wikberg *et al.* 2017).

Methods

Thermogravimetric analysis

The thermogravimetric analysis (TGA) of the biochars and the chemically impregnated biochars were performed using a thermobalance (DMT, Essen, Germany) under N_2 with a temperature range of 240 to 800 °C. The weight loss was monitored as a function of temperature to determine the temperature area where the highest weight loss occurs.

Activation methods

The biochars were activated both physically and chemically (Fig. 1). The physical activation was conducted using CO_2 as activation gas; for chemical activations, KOH (Honeywell Riedel-de Haën, Seelze, Germany) and H_3PO_4 (BDH Prolabo, VWR International, Fontenay-sous-Bois, France) were used with a biochar to chemical impregnation ratio of 1:3 (w:w). The KOH impregnation was performed by heating and

stirring the mixture at 60 °C for 3 h, whereas for H_3PO_4 the mixture was heated at 85 °C for 2 h. After the impregnation, the biochar was dried at 105 °C before the activation process. The activation temperatures were 700 and 450 °C for KOH and H_3PO_4, respectively. The activation time of both chemical activations was 1 h; physical activation time was 2 h. All activations were performed in a tubular oven (Carbolite GHC 12/600 three zone furnace horizontal, Hope Valley, United Kingdom) that was purged with N_2 for 1 h before heating to ensure the absence of oxygen. The activation chemicals, gases, and conditions were selected based on the existing literature, supported by the thermal weight loss pre-experiments. The activation treatments of the impregnated biochars were performed under N_2 atmosphere. With KOH, the N_2 flow rate has a substantial effect on porosity development, with higher rates giving higher porosities (Lillo-Ródenas *et al.* 2001; Lozano-Castelló *et al.* 2001). The flow rate used in the KOH activation was the maximum rate achievable with the oven, 333 mL/min. In H_3PO_4 activations a flow rate of 40 mL/min was used. The flow rate of the CO_2 activation was kept low (50 mL/min) to ensure activation proceeds through chemical control and any diffusional limitations are kept to minimum (Linares-Solano *et al*. 2000). After the activation, the chemically treated ACs were washed with water until near-neutral pH. To ease the removal of chemicals from the micropores, the ACs were dried at 105 °C between washing cycles, as water evaporation from the pores helps remove the chemicals dissolved in water. After the washings, the ACs were dried at 105 °C and weighed.

Adsorption tests

The adsorption experiments were used to investigate the effect of surface area, porosity, and pH on the adsorption capacity of selected ACs using two dyes: cationic methylthioninium chloride (methylene blue, MB) (Merck, Darmstadt, Germany) and anionic 4-(2-Hydroxy-1-naphthylazo)benzenesulfonic acid sodium salt (acid orange II, OII) (Merck), and one metal (zinc, Zn) (Merck). Willow was selected as the experimental plant due to the range of pH values (3.9 to 9.5) it has within the AC series. HTC-SPB-H_3PO_4 was also included in the test due to its ultrahigh surface area and pore volume. Adsorption of dyes was selected in order to gain insight on the suitability of the ACs for the removal of mesoscale (2 to 50 nm) organic molecules.

The ACs were tested for their adsorptive properties using adsorption of the dyes MB and OII into the pores by the method described in the literature (Raposo and De La Rubia 2009). A solution containing 300 mg MB or OII per liter H_2O was prepared. After 100 mL of this solution was transferred into Erlenmeyer flasks 250 mL in volume, 100 mg of AC was added, and the solutions were continuously agitated for 24 h to achieve equilibrium between adsorption and desorption of the test dye. Portions of each solution were filtered and, if needed, diluted, and the absorbance of the solution was measured at 664 nm (MB) or 485 nm (OII) on a Shimadzu UV-1800 double-beam spectrophotometer (Kyoto, Japan). The concentration of the solution was calculated from a calibration line obtained with known concentrations of the dyes. The adsorbed mass per carbon was calculated using Eq. 1, and the percent of respective dye removed was calculated using Eq. 2,

$$q(\text{abs}) = (C_0 - C_t) \text{ x } V / m \quad (1)$$

$$\% \text{ removed} = (C_0 - C_t) / C_0 \quad (2)$$

where q(abs) is the mass adsorbed per mass unit carbon (mg g^{-1}), x is the multiplication

operation, C_0 is the initial concentration of the tested dye (300 mg l^{-1}), C_t is the measured concentration after 24 h, V is the volume of dye solution used, and m is the mass of the activated carbon used.

Adsorption capacity of zinc metal was tested with selected carbons. A solution containing 100 mg/L of Zn^{2+} metal ion was prepared; 25 mL of initial solution was transferred into Erlenmeyer flask with 5 g/L of AC. Because the pH of the prepared ACs differs, the pH of the solution was adjusted to 6.5 or 4.0 with 0.1 M HCl to prevent the formation of unwanted precipitate and to verify metal adsorption. After the pH adjustment solution were continuously agitated for 24 h. Portions of each solution were filtered, diluted, and the concentration of the metal in the solution was measured with atomic absorption spectroscopy (AAS) Perkin-Elmer AAnalyst 200 (Boston, MA, USA). Adsorption capacities of Zn-metal were calculated as previously, using Eqs. 1 and 2.

Characterization methods

Elemental analysis for C, H, N, S and O was performed using FLASH 2000 series analyzer (Thermo Scientific, Waltham, MA, USA), and the ash content gravimetrically after burning the samples at 550 °C for 23 h. The BET surface area and pore size distribution were determined with a Micromeritics ASAP 2020 analyzer (Norcross, GA, USA). Prior to measurements, portions of each sample (200 mg) were pretreated at low pressures (2 µm Hg) and high temperatures (140 °C) for 180 min to clean the surfaces. Adsorption isotherms were obtained by immersing sample tubes in liquid nitrogen (-197 °C) to obtain isothermal conditions. Nitrogen was added to the samples in small steps, and the resulting isotherms were obtained. Specific surface areas were calculated from adsorption isotherms according to the BET (Brunauer–Emmett–Teller) method (Brunauer *et al*. 1938). Pore size distributions were calculated using the BJH (Barrett–Joyner–Halenda) algorithm (Barrett and Joyner 1951) and the DFT (Seaton and Quirke 1989) function. With the setup of the instrument used, a Micromeritics ASAP 2020, pores down to 1.5 nm in diameter could be measured. The samples were also characterized by FTIR spectroscopy for their surface functional groups using Thermo Scientific Nicolet iS50 FT-IR (Waltham, USA) with attenuated total reflectance unit (ATR) (range 4000 to 400 cm^{-1}, 32 scans). The pH was determined by stirring 0.5 g of carbon with 50 mL of deionized water overnight after which the pH was measured using Metrohm 744 pH Meter (Herisau, Switzerland). Boehm titration (Boehm *et al.* 1964) was applied for characterizing the acidic functionalities on the carbon surfaces. Depending on the amount of carbon sample available, 0.75, 0.60, or 0.45 g of carbon was shaken for 24 h in 25, 20, or 15 mL of 0.05 M reaction base ($NaHCO_3$, Na_2CO_3, and NaOH, each in three replicates), respectively. Thereafter, the suspension was filtered and an aliquot of 10 mL of the solution was titrated with 0.05 M HCl. The inflection points in the titration curves were determined with the second-derivative method, after which the amount of surface functional groups were calculated from the difference between the reaction bases before and after the reaction (Kim *et al*. 2012).

Micrometer-scale porosity was imaged with x-ray microtomography. HTC-SPB-H_3PO_4 was selected for imaging due to its ultrahigh BET surface area. For comparison, non-activated HTC-SPB was imaged. The sample size in imaging was approximately 1 mm. X-ray tomography was conducted with Zeiss MicroXCT-400 device (Pleasanton, USA). In total 1600 projection images evenly distributed in full 360° with an exposure time of 12 s. With the selected magnification, pixel size was 566 nm. Source voltage was 40

kV, and source current was 250 μA. The 3D reconstruction was done with device manufacturer's XMReconstructor software. The resulting images were analysed for porosity and specific surface area (Vogel *et al*. 2010).

RESULTS AND DISCUSSION

The attained ACs are denoted in the text using the abbreviations given in Fig. 1; for example, SP-SPB-KOH refers to slow pyrolyzed scots pine bark biochar that has been chemically activated with KOH. Biochar refers to the non-activated, but thermochemically treated, biomass and AC to activated carbon. The activation conditions of these experiments were chosen based on TGA experiments and literature, and were therefore not optimized for any of the biochars used. Through optimization of surface areas, for instance, could be enhanced and the amounts of surface oxygen groups could also be different. The purpose of the current experiment was to compare the obtained ACs produced from different biomasses using two different pre-carbonization methods. As each selected activation method was performed under similar conditions for each biochar, differences in the results may reveal differences between the used pre-carbonization methods and the biomasses used. This information is important when selecting suitable biomass and pre-treatment for a specific AC application.

Porosity and Surface Area of the Activated Carbons

The activation methods produced different PSDs for the SP and HTC biochars (Table 1). For the SP biochars, the microporosity was increased with all activation methods. For HTC biochars porosity development was dependent on the activation method. Both H_3PO_4 and CO_2 activations increased the meso- and macroscale porosity of the HTC biochars but with KOH activation, mainly microporosity was increased. These differences with the PSDs are probably due to the different physical characteristics of the SP and HTC biochars, combined with different reaction mechanisms of the used activation chemicals. PSDs are meaningful in the potential AC application perspective. Microporosity is favorable for gas adsorption, but larger pores are also needed for the gas transport inside the micropores (Cui *et al*. 2004). However, the adsorption of organic molecules, such as dyes, requires larger mesoscale pores due to the larger molecule size (Rodríguez *et al*. 2009). In both cases, interconnectivity of the pores is also an important factor. Regarding developed surface areas, the lowest surface areas were obtained from the SP biochar activations and the highest from the HTC biochar activations. Phosphoric acid was the most efficient activation agent producing ultrahigh surface area of 3505 m^2/g for the HTC-SPB, although KOH also produced high surface areas above up to 1594 m^2/g for the SP-willow.

Table 1. BET Surface Areas and Pore Size Distributions of the Biochars and Activated Carbons

Biochar	Activation Method	BET Surface Area (m^2/g)	Pore Volume (%)			
			Micropore 1.5-2 nm	Mesopore 2-50 nm	Macropore >50 nm	Total (cm^3/g)
HTC willow	-	3.7	2%	72%	26%	0.028
HTC SPB		42.5	nd	82%	18%	0.207
SP willow		8.0	14%	71%	14%	0.012
SP SPB		19.4	na	na	na	na
HTC willow	H_3PO_4	1682	39%	48%	13%	1.06
HTC SPB		3505	46%	54%	nd	2.19
SP willow		376	90%	10%	nd	0.187
SP SPB		339	92%	8%	nd	0.126
HTC willow	KOH	966	94%	4%	2%	0.296
HTC SPB		748	95%	5%	nd	0.391
SP willow		1594	90%	10%	nd	0.569
SP SPB		1056	98%	2%	nd	0.397
HTC willow	CO_2	257	74%	17%	9%	0.125
HTC SPB		238	46%	48%	7%	0.164
SP willow		339	78%	20%	1%	0.147
SP SPB		347	91%	7%	1%	0.137

The pore size distributions were calculated using DFT (density function theory) algorithm. na, not analyzed; nd, not detected.

KOH activation

The KOH activated HTC biochars resulted also in high surface areas with similar pore volumes and PSDs as the KOH activated SP biochars, with the exception of HTC biochar produced from willow having some macropore development as well (Table 1). The pore volumes of the KOH activated SP biochars were approximately three times higher than the pore volumes of the H_3PO_4 activated SP biochars. KOH was clearly the best activator for the SP biochars.

Alkaline metal compounds are commonly used for coal or biochar activation, and they can produce large surface areas and highly microporous structures (Lozano-Castelló *et al*. 2001). Activation with KOH has been proposed to proceed as $6KOH + 2C \rightarrow 2K + 3H_2 + 2K_2CO_3$ (Lillo-Ródenas *et al*. 2003, 2007), where the reactivity of the precursor has been linked to the start of hydrogen evolution during heating. When hydrogen evolution begins earlier, the precursor is more reactive towards KOH. Lillo-Ródenas *et al*. (2007) studied the effect of precursors' nature on the resulting AC porosity with alkaline activation and used 20% weight loss as an indicator of the precursor reactivity. That is, the lower the

temperature at this weight loss, the higher the reactivity in the chemical activation reaction. Using the above described 20% weight loss to assess biochar reactivity in this study, the TGA curves of the KOH impregnated biochars showed SP willow to be the least reactive biochar (Fig. 2). This was expected, as the most reactive carbon atoms are already volatilized during pyrolysis and the remaining carbons hold better the structural order. Surprisingly, the most reactive appeared to be SP SPB biochar, which produced the second highest surface area and pore volume after SP willow. The reactivity should decrease with rising pre-carbonization temperature (Lillo-Ródenas *et al*. 2007). Therefore, HTC biochars, which did not have as high loss in their SOG activity and are therefore more prone to react with KOH, should have been the most reactive. The HTC biochars' TGA curves remained, however, between the SP biochars. The high reactivity with KOH was still marked, as there were analytical difficulties during the TGA measurement due to vigorous reaction of HTC biochars with KOH by foaming. These analytical difficulties may explain the surprising TGA result. During the activation, especially HTC SPB began to foam, which also contributed to the low yield of the AC. The TGA and activation results indicate that the activation conditions may not have been optimal for the HTC biochars, especially the KOH:biochar ratio may have been too large. Too high amount of KOH may have accelerated the reaction, causing larger structure dilation into meso- and macropore scale (Lozano-Castelló *et al.* 2001). This is supported by the larger proportion of mesopores in the HTC ACs compared to SP ACs. The surface areas were also lower for HTC biochars than for SP biochars. Regarding the biomass type, no clear differences between willow and SPB were observed, the biggest differences were caused by the pre-carbonization methods.

Phosphoric acid activation

Phosphoric acid is an efficient activator with fresh biomass, as it can be efficiently absorbed in the plant tissue and cells and it has been used as impregnation chemical in activation of various biomasses (Jagtoyen and Derbyshire 1998; Girgis and El-Hendawy 2002; Suárez-García *et al.* 2002; Soleimani and Kaghazchi 2007; Patnukao and Pavasant 2008). The acid hydrolyzes glycosidic linkages in polysaccharides and cleaves aryl ether bonds in lignin at low temperatures followed by crosslinking reactions causing structural stabilization and dilation (Jagtoyen and Derbyshire 1998). HTC biochars are produced in lower temperatures than SP biochars and can retain the biomass characteristics, *e.g.* morphology and surface oxygen groups, better than SP biochars (Kambo *et al*. 2015). For this reason, HTC biochars are able to react with the impregnation chemical better than pyrolyzed biochars (Jain *et al.* 2016).

The suitability of H_3PO_4 for impregnation of HTC biochars is clear; the lowest surface area HTC willow biochar produced second highest surface area (1682 m^2/g), following HTC SPB biochar with the ultra-high surface area (3505 m^2/g).

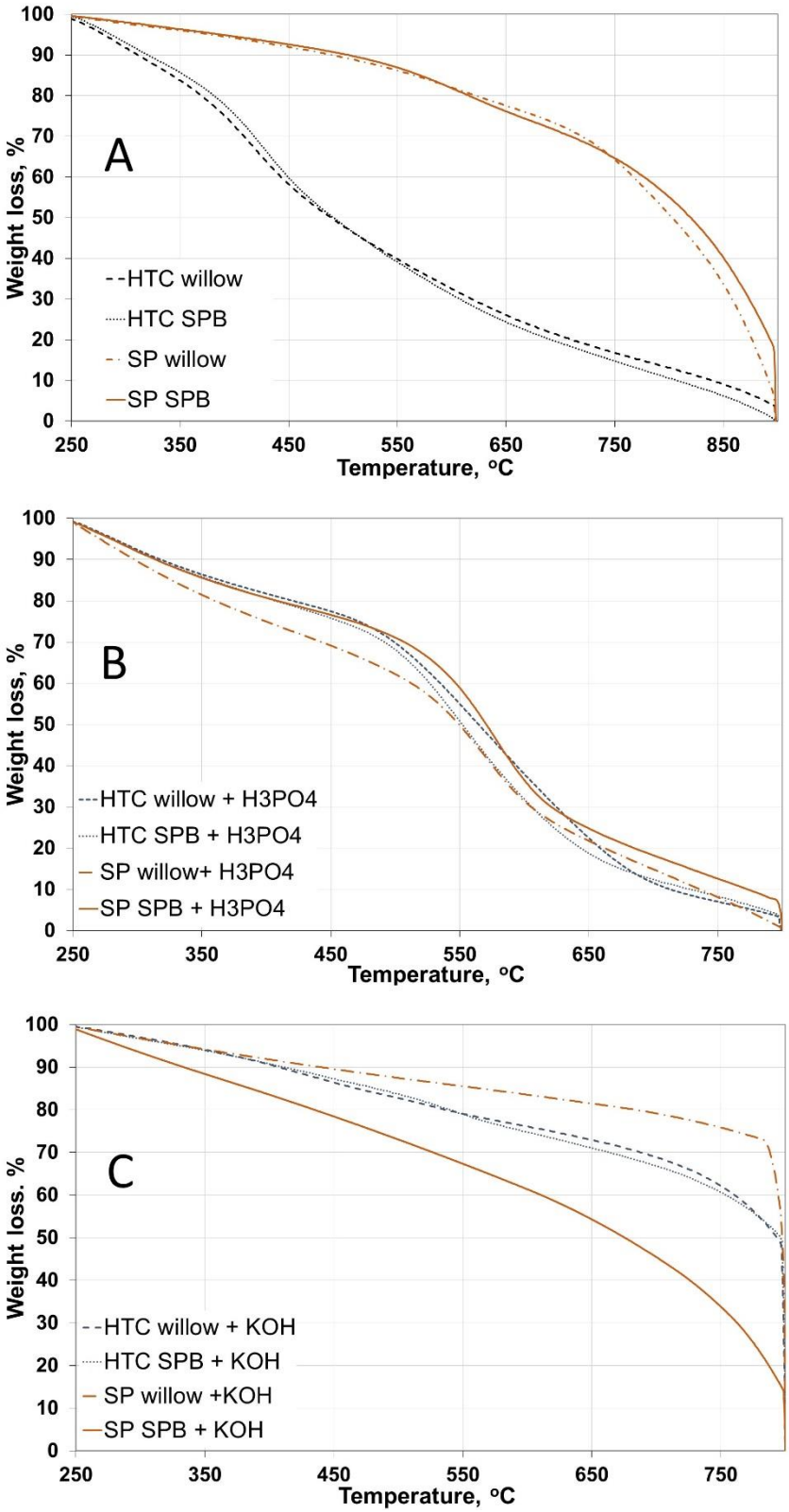

Fig. 2. Thermogravimetric curves of the biochars and chemically impregnated biochars. A: biochars as such; B: H_3PO_4 impregnated biochars; C: KOH impregnated biochars.

The much more stable and hard structure of SP biochars, combined with low porosity, can prevent the formation of rigid cross-linked structure inside the biochar particles and therefore the pore volumes and surface areas remain low. The used activation temperature (450 °C) may have also been too low: according to the TGA pre-experiments the fastest weight loss of the H_3PO_4 impregnated biochars occurred above 500 °C, although over 20 % weight loss was expected at the selected temperature. The activation weight loss was, however, only 2 to 4% with 90% of micropores and 10% mesopores (Tables 1 and 2). As a comparison, Teng *et al.* (1998) produced surface areas up to 854 m^2/g on bituminous coal with H_3PO_4 at 500 °C and 3 h, producing 80% micropores and 20% mesopores. One of their conclusion was that impregnation time need to be long enough and coal:acid ratio large enough for H_3PO_4 to enter the pore system, which may have been limiting factors in the present study preventing higher pore development. The TGA pre-experiment was not able to predict the weight loss behavior of pyrolyzed biochars during activation as accurately as HTC biochar behavior. Regarding biomass type, there were differences between HTC pre-carbonized willow and SPB, willow producing wider PSD. Willow produced the highest amount of macropores of all ACs in this study.

Physical activation

The physical activation with CO_2 produced the lowest surface areas and pore volumes (Table 1). The lowest surface areas and pore volumes were formed for the HTC biochars. The PSDs of all CO_2 ACs contained also macroporosity, which was not seen with the chemical activations apart from the exceptions of HTC-willow-H_3PO_4 and HTC-willow-KOH.

The physical activation showed no clear differences between the HTC and SP biochars, as both produced low surface areas and pore volumes. One reason may have been the activation time. Zhang *et al*. (2004) reported lower pore volumes for pyrolyzed corn hulls and corn stover using 800 °C and 2 h compared to 1 h duration. The same effect was not seen with oak char. They suggested that pore structure formation exceeded that of the destruction as a possible reason. Pore structure collapse could be a plausible reason for the lower surface areas and yields of HTC biochars, as the SP biochars were carbonized at 475 °C, resulting in much condensed and stable structure than that obtained through HTC at lower temperatures of 260 °C (Kambo *et al.* 2015). Therefore, SP biochars were able to form microporosity compared to HTC biochars, as can be seen from the yields and micropore volumes (Tables 1 and 2). The SP biochars could have possibly endured longer activation time and/or temperature and thereby develop larger surface area. The low surface areas of the HTC ACs were still surprising, as for example Hao *et al*. (2013) have reported surface areas of 489 to 749 m^2/g for CO_2 activated HTC biochars produced from various precursors in similar conditions. Willow produced similar PSDs with both pre-carbonization methods but with pine bark, the PSD was considerably wider with the HTC treated biochar. The surface areas of the H_3PO_4 activated and CO_2 activated SP biochars were quite similar.

Table 2. Yields, Elemental Composition, Ash Content, and pH of Biochars and Activated Carbons

Sample	Activation yield (%)	Total yield (%)	Elemental composition (%, mass based)					Ash (%)	pH
			O	C	H	N	S		
Biochars									
HTC willow	-	37	25 ± 0	70 ± 1	5.1 ± 0.0	0.63 ± 0.05	0 ± 0	1.1	4.5
HTC SPB	-	54	25 ± 0	69 ± 0	5.0 ± 0.1	0.28 ± 0.01	0 ± 0	2.1	4.4
SP willow	-	34	10 ± 0	78 ± 0	2.8 ± 0.0	0.81 ± 0.08	0 ± 0	6.9	6.9
SP SPB	-	40	9.8 ± 0.1	78 ± 4	2.7 ± 0.1	0.34 ± 0.02	0 ± 0	4.0	6.5
Activated carbons									
HTC willow H_3PO_4	69	25	9.0 ± 0.3	79 ± 7	2.5 ± 0.0	0.74 ± 0.09	0 ± 0	2.3	3.9
HTC SPB H_3PO_4	69	38	5.6 ± 0.1	83 ± 1	1.7 ± 0.0	0.22 ± 0.02	0 ± 0	2.6	4.0
SP willow H_3PO_4	98	33	5.6 ± 0.0	84 ± 1	2.0 ± 0.0	0.45 ± 0.03	0 ± 0	0.44	4.2
SP SPB H_3PO_4	96	39	8.5 ± 0.1	78 ± 1	2.6 ± 0.0	0.32 ± 0.01	0 ± 0	3.9	3.8
HTC willow KOH	45	16	11 **	86 ± 8	0.83 ± 0.1	0.26 ± 0.01	0 ± 0	2.7	6.2
HTC SPB KOH	26	14	6.5 ± 0.7	84 ± 1	0.66 ± 0.01	0.14 ± 0.00	0 ± 0	4.7	4.9
SP willow KOH	72	24	9.4 ± 0.3	84 ± 3	0.68 ± 0.07	0.05 ± 0.00	0 ± 0	3.9	7.2
SP SPB KOH	78	32	7.9 ± 0.2	83 ± 1	0.65 ± 0.03	0.15 ± 0.00	0 ± 0	5.9	5.2
HTC willow CO_2	52	19	1.3 ± 0.1	92 ± 2	0.68 ± 0.04	0.58 ± 0.06	0.04 ± 0.03*	2.5	5.4
HTC SPB CO_2	54	29	0.96 ± 0.02	91 ± 3	0.69 ± 0.01	0.25 ± 0.02	0 ± 0	4.1	6.8
SP willow CO_2	80	27	3.3 ± 0.4	84 ± 2	0.66 ± 0.01	0.63 ± 0.03	0 ± 0	7.3	9.5
SP SPB CO_2	81	33	2.0 ± 0.1	86 ± 4	0.70 ± 0.02	0.20 ± 0.01	0 ± 0	7.0	6.4

* most likely contamination during analysis; ** single determination

Surface Properties of the Biochars and Activated Carbons

The FTIR spectra for the biochars are presented in Fig. 3 and those for the ACs are in Fig. 4. There is clear difference in the spectra between the pre-treatments, HTC producing higher surface activity compared to SP. The peak around 1600 cm^{-1} (aromatic C=C streching in lignin) were found for both HTC and SP biochars, but peaks around 1450 cm^{-1} (C-H deformation in lignin and carbohydrates), 1270 and 1210 cm^{-1} (C-O stretching in lignin and xylan), and 1030 cm^{-1} (C-O stretching of carboxylic, ester and ether groups in cellulose and hemicellulose) (Labbé *et al.* 2006; Keiluweit *et al.* 2010) were clearly found only for HTC biochars. The biochar spectra of the HTC biochars showed alkyl peaks around 2929 and 2850 cm^{-1} appearing in area that has been found to correlate with hydrophobicity index of soil organic matter (Kinney *et al.* 2012). These peaks were completely missing from all SP biochars, as are the peaks around 1700 cm^{-1} (carboxyl C=O stretching) and 1510 cm^{-1} (C-H or N-H bending). The peak around 1510 cm^{-1} has been found to characterize undecomposed litter (Haberhauer *et al.* 1998), which reflects the raw biomass characteristics of HTC biochars. The differences between biomasses were also small. The only clear difference was the peak at 1115 cm^{-1} associated with aromatic skeletal and C-O stretching (Labbé *et al.* 2006) that was clearly present only in HTC willow biochar.

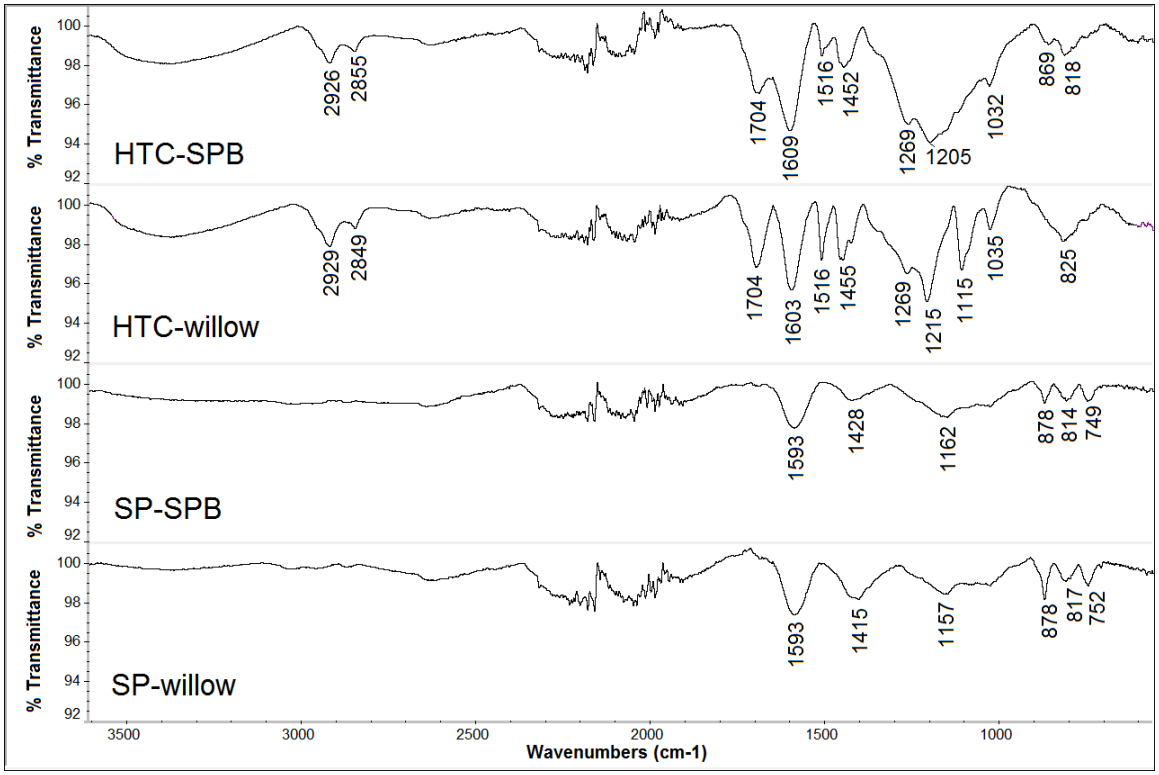

Fig. 3. FT-IR spectra of the biochars. Baseline corrected

The FTIR spectra of the activated carbons (Fig. 4) showed that chemical activation using H_3PO_4 produced the most surface-active ACs regarding the number of peaks and intensity. The CO_2 spectra resembled the KOH spectra with the amounts and peak locations. The SP-willow-CO_2 was the only one producing a strong peak at 1400 cm^{-1} of all activations (in-plane deformation of OH, Laginhas *et al.* 2016), which may partly explain its good performance in the adsorption tests (see section *Adsorption capacity*). The

H_3PO_4 ACs all have a strong peaks at 1590 to 1560 cm^{-1} (aromatic C=C stretching in lignin or conjugated C-O stretching) (Labbé *et al.* 2006) and ~1170-1160 cm^{-1} (C-O-C stretching of ester groups in cellulose and hemicellulose) (Keiluweit *et al.* 2010). The CO_2 and KOH ACs also have a peak around the same region but of much lower intensity than with the H_3PO_4 ACs. The CO_2 and KOH ACs had a medium or a strong peak at ~1030 cm^{-1} (C-O stretching of carboxylic, ester and ether groups). The disappearance of peak at 1030 cm^{-1} with H_3PO_4 is related to dehydration and depolymezation reactions during the activation (Jagtoyen and Derbyshire 1998; Keiluweit *et al.* 2010).

The effects of the HTC and SP pre-treatments were not that clear as they were with the biochars. The biggest differences were found between H_3PO_4 activated HTC- and SP-SPB biochars and KOH activated HTC- and SP-willow biochars. The differences between the biomasses were better seen with the activated HTC biochars, where willow produced slightly higher intensities compared to SPB ACs. With activated SP biochars, only H_3PO_4 activated willow had distinctly higher peak intensities compared to H_3PO_4 activated SPB.

Chemical activations produced or retained the most of surface oxygen groups (SOG) in the ACs. H_3PO_4 activation uses milder temperatures compared to KOH and CO_2 activations, which may be beneficial for preservation of carboxylic groups of the biochar, but it can cause structural changes in the biochar, which can lead to extensive growth in the size of aromatic units (Jagtoyen and Derbyshire 1998) including the polycyclic hydrocarbons (PAHs). The three-peak group at 874 to 750 cm^{-1} in the FTIR spectra, attributed to aromatic C-H bands found in PAHs (Lee and Choi 2000; Sandford *et al.* 2013) (Fig. 3) missing from the HTC biochar spectra, is clearly seen in all of the H_3PO_4 activated carbons, including the HTC ACs. The peak group seems to have disappeared from the CO_2 and KOH activated SP carbons, which, in contrast, points to a decrease in aromaticity. The appearance of PAHs in the ACs is clearly a negative aspect of the acid activation method, as PAH compounds are harmful and their amount is strictly regulated. However, the alkyl region 3000 to 2800 cm^{-1} connected to hydrophobicity (Kinney *et al*. 2012), disappeared from the HTC AC spectras and indicate loss of hydrophobicity from the HTC biochars due to activation.

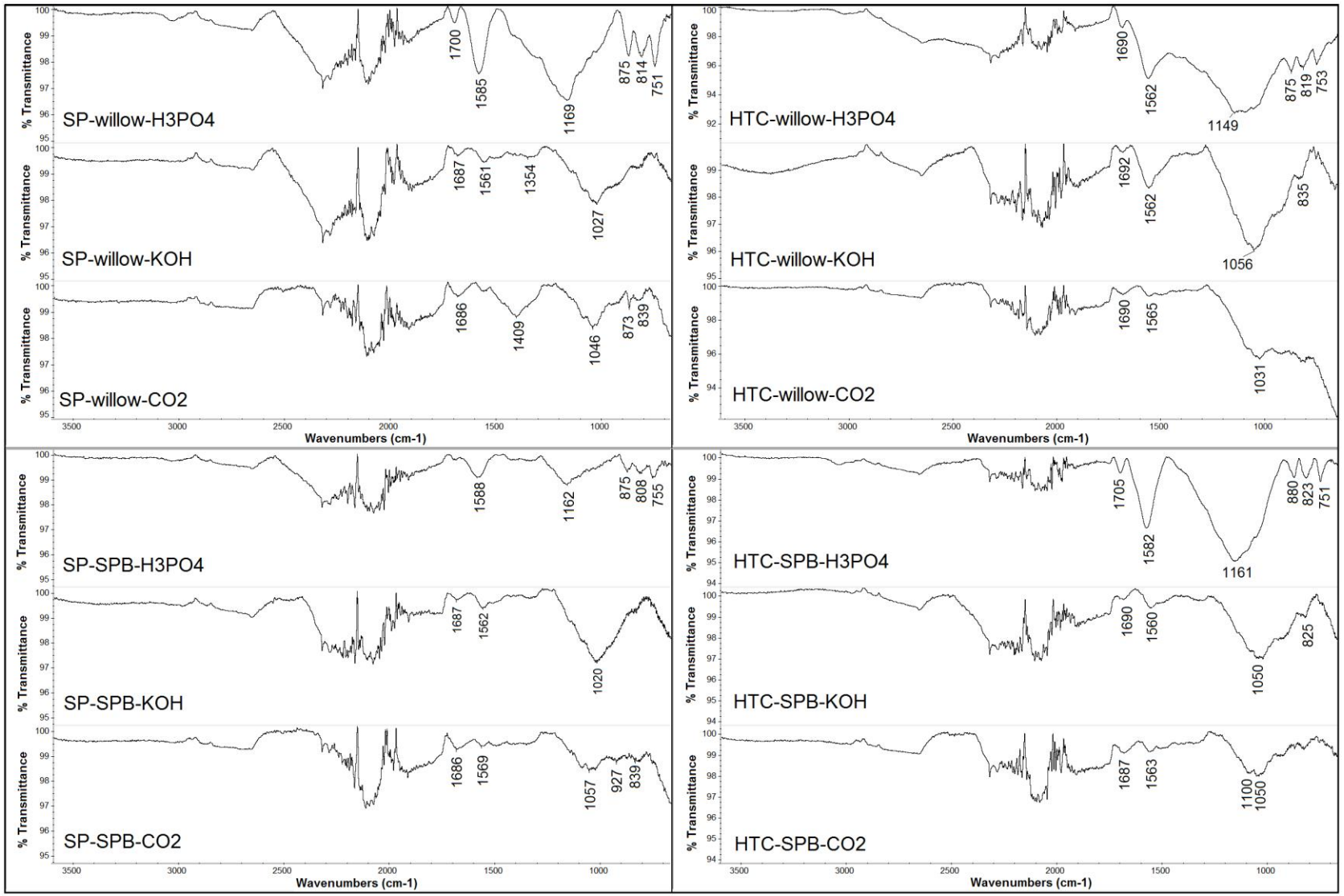

Fig. 4. FT-IR spectra of the activated carbons. Baseline corrected

The amount of SOGs can affect the ability of ACs to function as an adsorbent for different types of atoms and molecules, and their amount is therefore of interest. The chemically activated carbons had the largest quantities of surface activity while in physically activated carbons oxygen surface groups could not be detected (Table 3). Phosphoric acid ACs had rather even distribution of all oxygen groups, whereas lactonic groups dominate KOH ACs. Phenolic groups are missing from KOH activated SP-willow and from KOH activated HTC-SPB, as they could not be analyzed due to mobilization of interfering compounds during NaOH equilibration. This mobilization was evidenced by somewhat dark color of the extract and anomalous shape of the titration curve. The CO_2 ACs produced in higher temperature did not have a detectable amount of surface oxygen groups.

Table 3. Boehm Titration Results of the Surface Oxygen Groups

	Activation method	Groups			Total acidity (meq/g)
		Carboxyls (meq/g)	Lactones (meq/g)	Phenols (meq/g)	
HTC willow	H_3PO_4	0.17	0.11	0.21	0.49
HTC SPB		0.23	0.26	0.30	0.78
SP willow		0.27	0.20	0.13	0.61
SP SPB		0.21	0.14	0.16	0.50
HTC willow	KOH	0.14	0.36	0.17	0.67
HTC SPB		0.14	0.45	na	na
SP willow		0.15	0.54	0.00	0.69
SP SPB		0.14	0.31	0.18	0.63
HTC willow	CO_2	nd	nd	nd	nd
HTC SPB		nd	nd	nd	nd
SP willow		nd	nd	nd	nd
SP SPB		nd	nd	nd	nd

na, not analyzed; nd, not detected.

The Van Krevelen diagram can also be used to describe the reduction of oxygen and hydrogen in the carbonization process. The conversion proceeds gradually from the upper right corner of the diagram to lower left as the carbonization advances. The intensity of the carbonization is described by the distance of the dots. The increase in aromaticity due to activation is visible also in the Van Krevelen plot (Fig. 5) in the decreasing H/C ratios as the temperature rises. The decrease is most drastic with the activated HTC biochars where significant structural condensation occurs. The O/C ratios are in the same range for both chemical activations. Overall, activation using KOH and CO_2 caused slightly larger changes in both H/C and O/C ratios than activation using H_3PO_4 when compared to the biochars. The difference between the chemical activations is caused by the different activation mechanisms, where KOH promotes higher structural carbon stabilization by forming crystallites and removing crosslinking compared to H_3PO_4 activation mechanism (Moreno-Castilla *et al.* 2001). The loss of surface oxygen groups due to high activation temperature of CO_2 activation is also seen in Fig. 5.

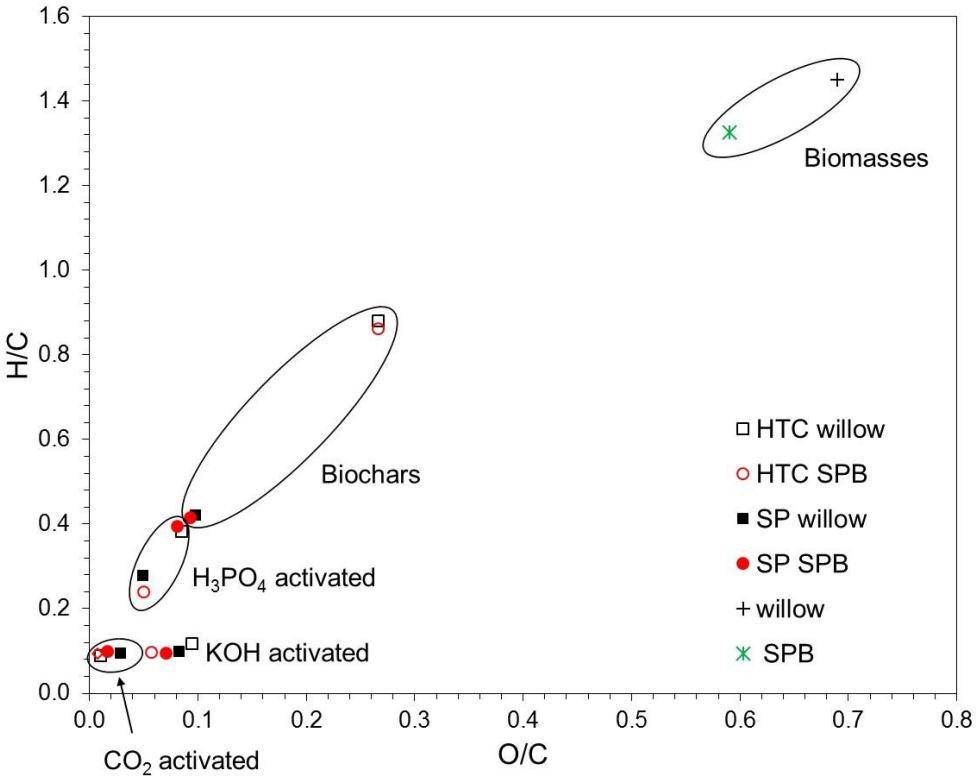

Fig. 5. The Van Krevelen plot of the biochars and the differently activated carbons

Yields and Chemical Composition

The activation yields from biochar to activated carbon varied between 26% and 98% being higher for SP biochars mainly due to the higher temperature used in the carbonization process, which causes volatilization of thermally less stable molecules already in the pre-carbonization stage (Table 2). Hence, the lower activation yields for HTC biochars are mostly due to the higher reduction of oxygen and hydrogen during activation. Especially with the KOH activation, the yields were low for the HTC biochars. This might partly be due to unoptimized activation conditions (see section KOH activation). The slightly lower yields of the KOH activated SP biochars are, on the other hand, caused by the surface area formation, as they had the highest surface areas of all SP ACs. The yields of H_3PO_4 activation were higher than those of KOH activation at all points, but also those of the physical activation. This is probably due to the different activation mechanisms, as KOH and CO_2 reaction are oxidative, but with H_3PO_4 the pore structure formation is based on the dehydration reactions and the occupation of the acid in the pores, which prevents destructuring (Romero-Anaya *et al*. 2012). With H_3PO_4 activation of willow biochars, the total activation yields are smaller than those of SPB, especially with HTC biochars. Despite the higher potential of HTC biochars to react with impregnation chemicals, the chemical activation did not result in equally high surface areas with KOH and H_3PO_4. It is clear from the results that the activation chemical had the highest impact on the surface area development. However, HTC biochars did produce considerably higher surface areas with both chemicals, whereas SP biochars reacted properly only with KOH, which was used with higher activation temperature. The total yields from biomass to biochar to activated carbon varied between 14% and 35%, being higher in general for SP biochars due to higher pre-carbonization yields combined with higher activations yields. Slightly higher yields

were observed for SPB than willow. The amount of ash was generally higher with ACs produced from the SP biochars. This arises from the HTC treatment, where part of the inorganics are leached from the biomass to the liquid phase and therefore not retained in the biochar (Funke and Ziegler 2010).

The amount of carbon in the ACs varies between 78% and 92%, being highest for CO_2 activated HTC biochars (Table 2). Differences between biochars regarding carbon content within activation methods are small and lost within the standard deviation. Bigger differences were found for oxygen content. SP biochars retained their oxygen better with the chemical activations, while with physical activations the amount of oxygen was drastically decreased. HTC biochars lost more oxygen than SP biochars with physical activation. Willow as raw material retained oxygen better than SPB, which is interesting, as willow and SPB biochars had the same initial oxygen content. The nitrogen contents were highest and of similar magnitude with the H_3PO_4 and CO_2 ACs. KOH activation produced low N contents for all ACs, the largest drop being from 0.81% to 0.05% with SP-willow-KOH. Overall, the N contents of the ACs reflected the original N contents of the biochars, and of the raw biomass. The biomass N contents were 0.4 and 0.3 % for willow and SPB, respectively (Wikberg *et al*. 2017). Apart from the SP-willow-KOH, willow ACs contained higher amounts of N than SPB.

Adsorption Capacity

The adsorption capacity was tested with activated carbons produced from willow biochar, as willow produced the widest range of AC pH values and with the H_3PO_4 activated biochar HTC SPB due to the ultrahigh surface area (Table 4). Adsorption capacity of the ACs is typically dependent on the surface area, pore volume, pore size distribution, and the surface chemistry. High surface areas increase the adsorption capacity and wide pore size distribution affects the ability of the molecules to enter the carbon pores. Methylene blue number is, in fact, traditionally used as an indicator of macro- and mesopore capacity (Raposo and De La Rubia 2009). Therefore, ACs with microporosity alone do not effectively adsorb MB, although the surface area might be high. All the tested ACs in this adsorption series had enough mesoscale porosity so that significant MB adsorption was possible. The adsorption capacities for MB ranged from 54 to 95 %.

The dye adsorption results show that surface area is the determining factor in adsorption (Table 4). Phosphoric acid activated HTC SBP with its ultrahigh surface area was the best adsorbent, reaching nearly 100% adsorption capacity with both dyes. HTC-willow-H_3PO_4 with much lower surface area reached the same or nearly the same capacity with both dyes as HTC-SPB-H_3PO_4, probably due to its wider pore size distribution with both meso- and macropores, allowing easier access for the dye molecules. SP-willow-KOH reached over 90% adsorption due to its high surface area.

MB as a cationic dye should perform best at higher pH and anionic OII in low pH (Rodríguez *et al.* 2009), but this effect was not clearly seen. As the pH of the dye solutions was not adjusted to any certain value prior the experiment, the AC pH influenced the solution pH and thereby the adsorption results. Of the three ACs with pH-values around 4, two performed well with OII with over 90% adsorption, but the third reached only 52%. The low performer was SP- willow-H_3PO_4 with very low surface area. Perhaps the most visible pH effect with OII can be seen between SP-willow-KOH (AC pH 7.2) and HTC-willow-H_3PO_4 (AC pH 3.9), where the latter AC had 28% larger adsorption capacity although their surface areas are almost the same. Then again, HTC- willow-H_3PO_4 had much larger mesopore volume, which may cause the difference in the results. With MB

there appeared to be some pH effect with the ACs having large surface areas but not so much with the low surface areas. Physically activated willow had the highest pH but adsorption barely exceeded 50% with both dyes.

The adsorption of Zn was again strongly dependent on the AC's pH and less dependent of the pore volume or surface area. The ACs having pH value above 6 were clearly the best performing adsorbents. The low pH phosphoric acid ACs were the least efficient adsorbents for Zn, and even the ultrahigh HTC-SPB-H_3PO_4 exhibited negligible adsorption capacity. The H_3PO_4 activated biochars were also tested using higher pH (6.5), but the adsorption capacities did not increase. The pH of the Zn-solutions did rise during the experiment but stayed below pH 6, apart from the SP-willow-CO_2, which had end-pH of 7.5 and the highest adsorption capacity. At pH-values above 7, Zn^{2+} is increasingly present as solid $Zn(OH)_2$ (Leyva Ramos *et al*. 2002); therefore part of the high adsorption capacity of SP-willow-CO_2 may be explained by $Zn(OH)_2$ precipitation. However, the Zn results confirm that BET surface area was not the only parameter affecting the sorption process. This is in agreement with the results of Abdelhadi *et al.* (2017), who produced biochar from olive mill waste and compared it with commercial activated carbon for heavy metal adsorption. The synthetized biochars had higher sorption capacity despite their lower surface area compared to the activated carbon.

The content of functional groups on the ACs affect the results as well. The correlations between the amount of different acidic surface groups and adsorption capacities (Table 5) revealed differences between the adsorbates. The phenolic group was the most influential SOG affecting the dye adsorption. MB correlated also with carboxylic and lactonic groups, which may partly explain its slightly higher capacities compared to OII. The lactonic group appeared to correlate most with the Zn adsorption; HTC-willow-KOH (Zn adsorption capacity 61%) contained three times higher concentration of lactone groups than HTC-willow-H_3PO_4 (Zn adsorption capacity 7%). The results confirm that activation with H_3PO_4 and KOH produce different content of SOGs on activated carbons, which may have strong influence in sorption applications. The effect of SOG activity could, however, only be analyzed for the chemically activated biochars, as for the CO_2 activated biochars acidic activity could not be detected with the used titration method.

Table 4. Adsorption Capacities of Selected Activated Carbons

Sample	MB	OII	Zn	AC pH
HTC willow H_3PO_4	92 %	95 %	7 %	3.9
HTC SPB H_3PO_4	95 %	95 %	9 %	4.0
SP willow H_3PO_4	62 %	52 %	5 %	4.2
HTC willow CO_2	55 %	47 %	13 %	5.4
HTC willow KOH	80 %	50 %	61 %	6.2
SP willow KOH	91 %	67 %	88 %	7.2
SP willow CO_2	54 %	52 %	98 %	9.5

Note: the pH of the dye adsorption was not adjusted; Zn adsorption was performed at pH 4.

Table 5. The Pearson's Correlation Coefficients between the Amount of Acidic Surface Groups and Adsorption Capacity

Correlation	MB	OII	Zn
Carboxylic groups	0.57	0.47	-0.48
Lactonic groups	0.63	0.11	0.36
Phenolic groups	0.80	0.70	-0.56
Total acidity	0.80	0.48	-0.15

Comparing adsorption capacity results across studies is somewhat challenging, as the results are affected by multiple factors, such as the adsorbate and adsorbent concentrations, pH, temperature, time, and competing ions. For reference, Kolodynska *et al* (2017) compared biochar (BET surface area 115.5 m^2/g) obtained from gasification process with commercial AC (Purolite 20, BET surface area 759.9 m^2/g) in adsorption of various heavy metals. Their results showed much higher Zn adsorption capacities for the biochar (18.6 mg/g) than for the AC (8.5 mg/g) at initial pH 5 and Zn concentration 100 mg/L. Kalavathy *et al.* (2010) studied Ni and Zn adsorption on H_3PO_4 AC prepared from rubber wood saw dust (BET surface area 1673.9 m^2/g, methylene blue number 255, pH 6 (Kalavathy *et al*. 2005)). The maximum adsorption capacity for Zn was found to be 22.0 mg/g. The three best performing ACs in the current study adsorbed 13.5 (HTC willow KOH), 19.1 (SP willow KOH), and 21.5 (SP willow CO_2) mg/g of Zn. The adsorption performances of the ACs are therefore similar to those in literature, although the experiment conditions were not identical. Dye removal capacities for MB have ranged from 90 mg/g to 683 mg/g using various waste biomasses as AC precursors and same activation reagents as in current study (González-García 2018). Zhang *et al.* (2007) tested activated carbon produced from coconut shells (BET surface area 799 m^2/g, pH 5.2) for OII adsorption acquiring adsorption capacity of 404 mg/g. The MB adsorption capacities of this study ranged from 161 to 286 mg/g and the OII capacities from 140 to 286 mg/g. The results are therefore in the range of those found in literature.

Overall, all the ACs were suitable for dye adsorption, regardless of the pore volume or the AC pH and the higher pH ACs for Zn adsorption, but clearly the results depend on the surface oxygen groups as well.

Micrometer-scale Pore Structure

X-ray microtomography and image analysis were utilized to observe possible changes in biochar sceleton structure due to activation. Visualizations of the images samples are shown in Fig. 6. The porosity obtained image analysis were 0.68 and 0.70 and specific surface area 103 and 109 mm^2/mm^3 for the activated and non-activated sample, respectively. For comparison, corresponding values for different biochars can be found from Hyväluoma *et al*. (2017). As gas adsorption measurements are limited to pores smaller than a few hundred nanometers, a majority of the total porosity cannot be detected with this method. However, larger pores are important as means of transport, providing pathways for the adsorbate from the surfaces to the adsorption sites at the interior parts of biochar particles. Thus it would be important to know whether activation influences the micrometer-scale porosity and pore connectivity. Because HTC-SPB-H_3PO_4 had the highest BET surface area, this AC and its non-activated counterpart were selected for imaging.

Imaging is able to discern only that part of surface area, which is visible at the used

imaging resolution. In spite of the ultrahigh surface area of the activated sample, the surface areas calculated from the images indicate that activation did not have any noticeable effect on the micrometer-scale porosity. The porosity and specific surface area of the activated and nonactivated SPB samples were very close to each other and in the same range as those determined earlier for various biochars in Hyväluoma *et al.* (2017). The micrometer scale pores of the activated SPB sample can be characterized as large cavities with size up to *ca.* 70 µm. These cavities did not have micrometer-sized connections and thereby did not provide fast transport pathways to inner parts of biochar particles. Thus, sorption sites in the inner parts may be more slowly accessible than those on the particle surfaces. Non-activated willow biochar used in the present work was imaged in a previous study by Hyväluoma *et al.* (2017) who found it to have pore structure consisting of straight tubular pores oriented in a parallel manner. It could thus be hypothetized that the biochar skeleton and transport taking place in micrometer-scale pores might affect the functions of ACs in different environments. X-ray microtomography and image analysis revealed that H_3PO_4-activation did not affect the micrometer-scale pore structure of HTC-SPB and thus these functions can be influenced only via raw material selection.

The interpretation of the obtained physical properties in the ACs requires information about the original pore structure of the raw biomass. The SPB raw material used here was of "practical quality" and originated from an industrial process. The same material was used in a previous study (Hyväluoma *et al.* 2017), where this material was found to be heterogeneous due to robust debarking method and contained also stemwood in addition to the actual bark. If macroporosity is desirable in the resulting AC, then the selected precursor biochar needs to contain macropores already before activation. The best activation results probably could be achieved if the activation method (biochar:chemical ratio, temperature, time, *etc*.) is optimized with the biomass pore structure, but the heterogeneity of especially waste biomass does clearly pose a challenge.

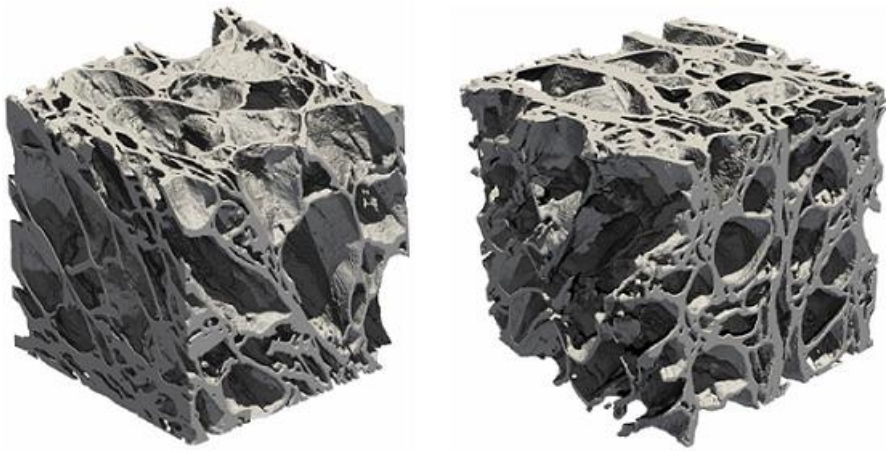

Fig 6. 3D reconstructions of the pore structure of HTC-SPB (left) and HTC-SPB-H_3PO_4 (right)

Potential Applications for the Bio-Based ACs

The amount of research conducted on various electrochemical applications suitable for activated biochars has been increasing during recent years. The interest rises from the need to develop environmentally friendly materials with low costs and high performance (Sevilla and Mokaya 2014). Activated carbons have traditionally been used in water and gas purification applications, of which water purification was also tested in this study.

Recent advances in the ability to tailor the porous structure of the ACs have shifted the focus to the development of, for example, electrode materials and hydrogen storages that may require highly specific PSDs. Activated carbons produced from various waste biomasses have been shown to perform extremely well in these types of applications (Munnings *et al*. 2014; Fuertes and Sevilla 2015; Pang *et al*. 2016). Supercapacitors have proven to be highly potential target application for HTC based ACs specific capacitances exceeding the values of commercially available supercapacitors (Sevilla and Mokaya 2014; Fuertes and Sevilla 2015). Supercapacitors benefit from narrow PSD consisting of micro- and mesopores, which is difficult to obtain through physical activation. Chemical activation can be used to tailor the PSD by altering impregnation ratios, activation temperatures and time, as discovered also from the results of this study. The ACs produced in this study possess qualities suitable for supercapacitors. Phosphoric acid activation of the HTC biochars have produced PSDs with equal amounts of micro- and mesopores, in addition to high surface areas. One interesting difference between the activated carbons was the amount of nitrogen. The amount of nitrogen may be highly interesting factor when considering electrochemical applications, which benefit from nitrogen. In some cases, nitrogen has been doped to the carbon structure for example by adding melamine in the activation chemical mixture (Fuertes and Sevilla 2015). Selection of raw materials that originally contain high amount of nitrogen may produce ACs with good performance without any extra doping. Phosphoric acid activated HTC willow had 0.74% of nitrogen in the structure (Table 2). As a comparison, Fuertes and Sevilla (2015) have produced nitrogen-doped KOH activated HTC biochar from sawdust having 1.3% of nitrogen (AC without N-doping had N content of 0.1%). Willow, exhibiting seven times higher amount of nitrogen compared to sawdust and comparable nitrogen amount to the N-doped sawdust, makes it an interesting raw material candidate for this type of ACs.

CONCLUSIONS

1. Chemical and physical characteristics of activated carbons depend on all the following variables: raw material type, pre-carbonization process, and most of all the selection of activation method. Regarding surface area development, both tested chemical activations were suitable for the HTC biochars, H_3PO_4 being the most suitable. For slow pyrolyzed biochars, only KOH activation produced adequate results. CO_2 was the least efficient activator for all biochars.
2. The pore size distributions also varied considerably between the activations, where KOH produced highly microporous ACs, whereas with H_3PO_4 and CO_2 wider pore size distributions were obtained. Only HTC willow biochars produced macroporosity with chemical activations.
3. The effect of the original pore size distribution on the results was also seen to have an effect. Chemical activation using H_3PO_4 did not affect macropore structure of the SPB activated carbon.
4. All the tested activated carbons were suitable for dye adsorption, but high surface area H_3PO_4 activated HTC biochars were clearly the best performers. Zinc adsorption was dependent on the pH of the ACs but also on the amount of lactonic surface oxygen groups.

ACKNOWLEDGMENTS

The authors thank the personnel at VTT for all the help provided with the analytical measurements, Mirja Muhola for performing the thermogravimetrical experiments, and M.Sc. Heimo Kanerva for performing the HTC experiments. Prof. Sylvia Larsson and Gunnar Kalén from SLU (Swedish University of Agricultural Sciences) are warmly thanked for providing the biomasses. This project has received funding from the European Union's Horizon 2020 Research and Innovation Programme under grant agreement No 637020-MOBILE FLIP.

REFERENCES CITED

Abdelhadi, S. O., Dosoretz, C. G., Rytwo, G., Gerchman, Y., and Azaizeh, H. (2017). "Production of biochar from olive mill solid waste for heavy metal removal," *Bioresource Technology* 244, 759-767. DOI: 10.1016/J.BIORTECH.2017.08.013

Barrett, E.P., Joyner, L.G., and Halenda, P. P. (1951). "The determination of pore volume and area distributions in porous substances. I. Computations from nitrogen isotherms," *Journal of the American Chemical Society* 73(1), 373-380. DOI: 10.1021/ja01145a126

Basta, A. H., Fierro, V., El-Saied, H., and Celzard, A. (2009). "2-Steps KOH activation of rice straw: An efficient method for preparing high-performance activated carbons," *Bioresource Technology* 100(17), 3941-3947. DOI: 10.1016/J.BIORTECH.2009.02.028

Boehm, H.-P., Diehl, E., Heck, W., and Sappok, R. (1964). "Surface oxides of carbon," *Angewandte Chemie International Edition* 3(10), 669-677. DOI: 10.1002/anie.196406691

Brunauer, S., Emmett, P. H., and Teller, E. (1938). "Adsorption of gases in multimolecular layers," *Journal of the American Chemical Society* 60(2), 309-319. DOI: 10.1021/ja01269a023

Cai, W., Zhou, Q., Xie, Y., Liu, J., Long, G., Cheng, S., and Liu, M. (2016). "A direct carbon solid oxide fuel cell operated on a plant derived biofuel with natural catalyst," *Applied Energy* 179, 1232-1241. DOI: 10.1016/j.apenergy.2016.07.068

Cui, X., Bustin, R. M., and Dipple, G. (2004). "Selective transport of CO_2, CH_4, and N_2 in coals: Insights from modeling of experimental gas adsorption data," *Fuel* 83(3), 293-303. DOI: 10.1016/J.FUEL.2003.09.001

Falco, C., Marco-Lozar, J. P., Salinas-Torres, D., Morallón, E., Cazorla-Amorós, D., Titirici, M. M., and Lozano-Castelló, D. (2013). "Tailoring the porosity of chemically activated hydrothermal carbons: Influence of the precursor and hydrothermal carbonization temperature," *Carbon* 62, 346-355. DOI: 10.1016/j.carbon.2013.06.017

Fuertes, A. B., and Sevilla, M. (2015). "Superior capacitive performance of hydrochar-based porous carbons in aqueous electrolytes," *ChemSusChem* 8(6), 1049-1057. DOI: 10.1002/cssc.201403267

Funke, A., and Ziegler, F. (2010). "Hydrothermal carbonization of biomass: A summary and discussion of chemical mechanisms for process engineering," *Biofuels, Bioproducts and Biorefining* 4(2), 160-177. DOI: 10.1002/bbb.198

Girgis, B. S., and El-Hendawy, A.-N. A. (2002). "Porosity development in activated carbons obtained from date pits under chemical activation with phosphoric acid," *Microporous and Mesoporous Materials* 52(2), 105-117. DOI: 10.1016/S1387-1811(01)00481-4

González-García, P. (2018). "Activated carbon from lignocellulosics precursors: A review of the synthesis methods, characterization techniques and applications," *Renewable and Sustainable Energy Reviews* 82, 1393-1414. DOI: 10.1016/J.RSER.2017.04.117

Haberhauer, G., Rafferty, B., Strebl, F., and Gerzabek, M. H. (1998). "Comparison of the composition of forest soil litter derived from three different sites at various decompositional stages using FTIR spectroscopy," *Geoderma* 83(3-4), 331-342. DOI: 10.1016/s0016-7061(98)00008-1

Hao, W., Björkman, E., Lilliestråle, M., and Hedin, N. (2013). "Activated carbons prepared from hydrothermally carbonized waste biomass used as adsorbents for CO_2," *Applied Energy* 112, 526-532. DOI: 10.1016/j.apenergy.2013.02.028

Hyväluoma, J., Kulju, S., Hannula, M., Wikberg, H., Källi, A., and Rasa, K. (2017). "Quantitative characterization of pore structure of several biochars with 3D imaging," *Environmental Science and Pollution Research*. DOI: 10.1007/s11356-017-8823-x

Ioannidou, O., and Zabaniotou, A. (2007). "Agricultural residues as precursors for activated carbon production – A review," *Renewable and Sustainable Energy Reviews* 11(9), 1966-2005. DOI: 10.1016/j.rser.2006.03.013

Jagtoyen, M., and Derbyshire, F. (1998). "Activated carbons from yellow poplar and white oak by H_3PO_4 activation," *Carbon* 36(7-8), 1085-1097. DOI: 10.1016/S0008-6223(98)00082-7

Jain, A., Balasubramanian, R., and Srinivasan, M. P. (2016). "Hydrothermal conversion of biomass waste to activated carbon with high porosity: A review," *Chemical Engineering Journal* 283, 789-805. DOI: 10.1016/j.cej.2015.08.014

Kalavathy, H., Karthik, B., and Miranda, L. R. (2010). "Removal and recovery of Ni and Zn from aqueous solution using activated carbon from *Hevea brasiliensis*: Batch and column studies," *Colloids and Surfaces B: Biointerfaces* 78(2), 291-302. DOI: 10.1016/J.COLSURFB.2010.03.014

Kalavathy, M. H., Karthikeyan, T., Rajgopal, S., and Miranda, L. R. (2005). "Kinetic and isotherm studies of Cu(II) adsorption onto H_3PO_4-activated rubber wood sawdust," *Journal of Colloid and Interface Science* 292(2), 354-362. DOI: 10.1016/J.JCIS.2005.05.087

Kambo, H. S., and Dutta, A. (2015). "A comparative review of biochar and hydrochar in terms of production, physico-chemical properties and applications," *Renewable and Sustainable Energy Reviews* 45, 359-378. DOI: 10.1016/J.RSER.2015.01.050

Keiluweit, M., Nico, P. S., Johnson, M. G., and Kleber, M. (2010). "Dynamic molecular structure of plant biomass-derived black carbon (Biochar)," *Environmental Science & Technology* 44(4), 1247-1253. DOI: 10.1021/es9031419

Keskinen, R., Hyväluoma, J., Wikberg, H., Källi, A., Salo, T., and Rasa, K. (2017). "Possibilities of using liquids from slow pyrolysis and hydrothermal carbonization in acidification of animal slurry," *Waste and Biomass Valorization*. DOI: 10.1007/s12649-017-9910-4

Kim, Y. S., Yang, S. J., Lim, H. J., Kim, T., and Park, C. R. (2012). "A simple method for determining the neutralization point in Boehm titration regardless of the CO_2

effect," *Carbon*, Pergamon 50(9), 3315-3323. DOI: 10.1016/J.CARBON.2011.12.030

Kinney, T. J., Masiello, C. A., Dugan, B., Hockaday, W. C., Dean, M. R., Zygourakis, K., and Barnes, R. T. (2012). "Hydrologic properties of biochars produced at different temperatures," *Biomass and Bioenergy* 41, 34-43. DOI: 10.1016/j.biombioe.2012.01.033

Kołodyńska, D., Krukowska, J., and Thomas, P. (2017). "Comparison of sorption and desorption studies of heavy metal ions from biochar and commercial active carbon," *Chemical Engineering Journal* 307, 353-363. DOI: 10.1016/J.CEJ.2016.08.088

Labbé, N., Harper, D., Rials, T., and Elder, T. (2006). "Chemical structure of wood charcoal by infrared spectroscopy and multivariate analysis," *Journal of Agricultural and Food Chemistry* 54(10), 3492-3497. DOI: 10.1021/jf053062n

Laginhas, C., Nabais, J. M. V., and Titirici, M. M. (2016). "Activated carbons with high nitrogen content by a combination of hydrothermal carbonization with activation," *Microporous and Mesoporous Materials* 226, 125-132. DOI: 10.1016/j.micromeso.2015.12.047

Lee, S. H., and Choi, C. S. (2000). "Chemical activation of high sulfur petroleum cokes by alkali metal compounds," *Fuel Processing Technology* 64(1-3), 141-153. DOI: 10.1016/S0378-3820(00)00070-9

Leyva Ramos, R., Bernal-Jacome, L. A., Mendoza-Barron, J., Fuentes Rubio, L., and Guerrero-Coronado, R. M. (2002). "Adsorption of zinc(II) from an aqueous solution onto activated carbon," *Journal of Hazardous Materials* 90(1), 27-38. DOI: 10.1016/S0304-3894(01)00333-8

Lillo-Ródenas, M. A., Cazorla-Amorós, D., and Linares-Solano, A. (2003). "Understanding chemical reactions between carbons and NaOH and KOH," *Carbon* 41(2), 267-275. DOI: 10.1016/S0008-6223(02)00279-8

Lillo-Ródenas, M. A., Lozano-Castelló, D., Cazorla-Amorós, D., and Linares-Solano, A. (2001). "Preparation of activated carbons from Spanish anthracite: II. Activation by NaOH," *Carbon* 39(5), 751-759. DOI: 10.1016/S0008-6223(00)00186-X

Lillo-Ródenas, M. A., Marco-Lozar, J. P., Cazorla-Amorós, D., and Linares-Solano, A. (2007). "Activated carbons prepared by pyrolysis of mixtures of carbon precursor/alkaline hydroxide," *Journal of Analytical and Applied Pyrolysis* 80(1), 166-174. DOI: 10.1016/j.jaap.2007.01.014

Linares-Solano, A., Salinas-Martínez de Lecea, C., Cazorla-Amorós, D., and Martín-Gullón, I. (2000). "Porosity development during CO_2 and steam activation in a fluidized bed reactor," *Energy & Fuels* 14(1), 142-149. DOI: 10.1021/ef9900637

Lozano-Castelló, D., Lillo-Ródenas, M. A., Cazorla-Amorós, D., and Linares-Solano, A. (2001). "Preparation of activated carbons from Spanish anthracite: I. Activation by KOH," *Carbon* 39(5), 741-749. DOI: 10.1016/S0008-6223(00)00185-8

Marsh, H., and Rodríguez-Reinoso, F. (2006). *Activated Carbon*, Elsevier Science, Amsterdam, Netherlands.

Moreno-Castilla, C., Carrasco-Marín, F., López-Ramón, M. V., and Alvarez-Merino, M. A. (2001). "Chemical and physical activation of olive-mill waste water to produce activated carbons," *Carbon* 39(9), 1415-1420. DOI: 10.1016/S0008-6223(00)00268-2

Munnings, C., Kulkarni, A., Giddey, S., and Badwal, S. P. S. (2014). "Biomass to power conversion in a direct carbon fuel cell," *International Journal of Hydrogen Energy* 39(23), 12377-12385. DOI: 10.1016/j.ijhydene.2014.03.255

Pang, L., Zou, B., Zou, Y., Han, X., Cao, L., Wang, W., and Guo, Y. (2016). "A new route for the fabrication of corn starch-based porous carbon as electrochemical supercapacitor electrode material," *Colloids and Surfaces A: Physicochemical and Engineering Aspects* 504, 26-33. DOI: 10.1016/j.colsurfa.2016.05.049

Patnukao, P., and Pavasant, P. (2008). "Activated carbon from *Eucalyptus camaldulensis* Dehn bark using phosphoric acid activation," *Bioresource Technology* 99(17), 8540-8543. DOI: 10.1016/j.biortech.2006.10.049

Raposo, F., De La Rubia, M. A., and Borja, R. (2009). "Methylene blue number as useful indicator to evaluate the adsorptive capacity of granular activated carbon in batch mode: Influence of adsorbate/adsorbent mass ratio and particle size," *Journal of Hazardous Materials* 165(1-3), 291-299. DOI: 10.1016/j.jhazmat.2008.09.106

Rodríguez, A., García, J., Ovejero, G., and Mestanza, M. (2009). "Adsorption of anionic and cationic dyes on activated carbon from aqueous solutions: Equilibrium and kinetics," *Journal of Hazardous Materials* 172(2-3), 1311-1320. DOI: 10.1016/j.jhazmat.2009.07.138

Romero-Anaya, A. J., Lillo-Ródenas, M. A., Salinas-Martínez de Lecea, C., and Linares-Solano, A. (2012). "Hydrothermal and conventional H_3PO_4 activation of two natural bio-fibers," *Carbon* 50(9), 3158-3169. DOI: 10.1016/j.carbon.2011.10.031

Sandford, S. A., Bernstein, M. P., and Materese, C. K. (2013). "The infrared spectra of polycyclic aromatic hydrocarbons with excess peripheral H atoms (H n -PAHs) and their relation to the 3.4 and 6.9 μm PAH emission features," *The Astrophysical Journal Supplement Series* 205(1), 8. DOI: 10.1088/0067-0049/205/1/8

Seaton, N. A., Walton, J. P. R. B., and Quirke, N. (1989). "A new analysis method for the determination of the pore size distribution of porous carbons from nitrogen adsorption measurements," *Carbon* 27(6), 853-861. DOI: 10.1016/0008-6223(89)90035-3

Sevilla, M., and Mokaya, R. (2014). "Energy storage applications of activated carbons: supercapacitors and hydrogen storage," *Energy & Environmental Science* 7(4), 1250-1280. DOI: 10.1039/C3EE43525C

Soleimani, M., and Kaghazchi, T. (2007). "Agricultural waste conversion to activated carbon by chemical activation with phosphoric acid," *Chemical Engineering & Technology* 30(5), 649-654. DOI: 10.1002/ceat.200600325

Suárez-García, F., Martínez-Alonso, A., and Tascón, J. M. (2002). "Pyrolysis of apple pulp: chemical activation with phosphoric acid," *Journal of Analytical and Applied Pyrolysis* 63(2), 283-301. DOI: 10.1016/S0165-2370(01)00160-7

Teng, H., Yeh, T.-S., and Hsu, L.-Y. (1998). "Preparation of activated carbon from bituminous coal with phosphoric acid activation," *Carbon* 36(9), 1387-1395. DOI: 10.1016/S0008-6223(98)00127-4

Vogel, H.-J., Weller, U., and Schlüter, S. (2010). "Quantification of soil structure based on Minkowski functions," *Computers & Geosciences* 36(10), 1236-1245. DOI: 10.1016/J.CAGEO.2010.03.007

Wikberg, H., Grönberg, J., Jermakka, J., Kemppainen, K., Kleen, M., Laine, C., Paasikallio,V., and Oasmaa, A. (2015a). "Hydrothermal refining of biomass - An overview and future perspectives," *Tappi Journal* 14(3), 195–207.

Wikberg, H., Grönqvist, S., Niemi, P., Mikkelson, A., Siika-aho, M., Kanerva, H., Käsper, A., and Tamminen, T. (2017). "Hydrothermal treatment followed by enzymatic hydrolysis and hydrothermal carbonization as means to valorise agro- and forest-based biomass residues," *Bioresource Technology* 235, 70-78. DOI:

10.1016/j.biortech.2017.03.095

Wikberg, H., Ohra-aho, T., Pileidis, F., and Titirici, M.-M. (2015). "Structural and morphological changes in kraft lignin during hydrothermal carbonization," *ACS Sustainable Chemistry & Engineering* 3(11), 2737-2745. DOI: 10.1021/acssuschemeng.5b00925

Yahya, M. A., Al-Qodah, Z., and Ngah, C. W. Z. (2015). "Agricultural bio-waste materials as potential sustainable precursors used for activated carbon production: A review," *Renewable and Sustainable Energy Reviews* 46, 218-235. DOI: 10.1016/j.rser.2015.02.051

Zhang, T., Walawender, W., Fan, L., Fan, M., Daugaard, D., and Brown, R. (2004). "Preparation of activated carbon from forest and agricultural residues through CO activation," *Chemical Engineering Journal* 105(1-2), 53-59. DOI: 10.1016/j.cej.2004.06.011

Zhang, G., Qu, J., Liu, H., Cooper, A. T., and Wu, R. (2007). "$CuFe_2O_4$/activated carbon composite: A novel magnetic adsorbent for the removal of acid orange II and catalytic regeneration," *Chemosphere* 68(6), 1058-1066. DOI: 10.1016/J.CHEMOSPHERE.2007.01.081

Article submitted: April 18, 2018; Peer review completed: May 31, 2018; Revisions received and accepted: June 12, 2018; Published: June 15, 2018.
DOI: 10.15376/biores.13.3.5976-6002